Accurate and Robust Skin Feature Extraction Scheme for Aging Estimation

Hyungjoon Kim, Jisoo Park, Eenjun Hwang
School of Electrical Engineering
Korea University
Anam-Dong, Seongbuk-Gu, Seoul, Republic Korea
E-mail: {hyungjun89, jisoo_park, ehwang04}@korea.ac.kr

Woogeol Kim
VC Smart Validation Team
LG Electronics
Pyeongtaek, Republic Korea
E-mail: woogeol.kim@lge.com

***Abstract*— In this paper, we revise our method for skin feature extraction based on cell segmentation to improve its accuracy, efficiency and robustness that are very critical in the realistic skin condition analysis. In order to achieve such goals, we enhance the contrast of wrinkles on the skin by using the contrast limited adaptive histogram equalization (CLAHE) and highlight the depth of wrinkles by using the extended-minima transform. By performing watershed transform, we can segment the skin image into labelled skin cells and calculate various skin features from the labelled cells. We focus on two types of skin features that play a key role in assessing the degree of skin aging; cell features and wrinkle features. To evaluate the performance and robustness of our revised method, we collected skin images using three different types of microscopy cameras and extracted their cell and wrinkle features using the revised method. Through various experiments, we show that our revised method achieves 10% increase in the skin feature extraction accuracy and 50% decrease in the skin feature extraction time compared to our previous method.**

Keywords- Skin analysis; Feature extraction; Wrinkle feature; Contrast stretching; Microscopy image.

I. INTRODUCTION

In this paper, we reinforce the experimental part of our work [1] for skin feature extraction scheme. Various factors, such as exposure to sunlight or pollution, smoking and excessive drinking are known to accelerate the normal skin aging process and eventually lead to premature skin aging. Since skin is the outermost part of the human body, people have shown great interest in the beauty and health of their skin. This in return leads to diverse studies related to skin analysis, skin treatment, and skin aging. Usually, the degree of skin aging has been evaluated by dermatologists based on their personal experience or knowledge. This is because there is no standard method for quantitative and objective evaluation. If such method was available, then users would get consistent and quantitative information about their skin condition, and hence perform suitable treatment for their skin more effectively and conveniently.

In our previous work, we proposed a scheme for skin texture aging trend analysis based on diverse skin texture features such as texture length, width, depth, cell count and cell area. To extract such features, we cropped microscopy skin image, carried out histogram equalization, removed noise and then binarized the image using the Otsu threshold. After that, we segmented the skin texture into cells by using the watershed algorithm and calculated their features [2][3]. However, there are several problems in our previous work. Two serious problems among them are feature extraction time and feature extraction accuracy. The former is due to the fact that its feature extraction is pixel-based and hence all pixels in each cell should be considered. The latter is due to the fact that preprocessing steps in the previous work were optimized for a specific microscope camera. Hence, the feature extraction result might be not good when using other types of cameras.

In this paper, we modify some of the preprocessing steps and segmentation method in the previous work to improve the accuracy, efficiency and robustness of skin feature extraction. Figure 1 shows the overall steps to achieve that, which can be divided into preprocessing, cell segmentation and feature extraction. In the preprocessing, the original image is cropped to reduce the effect of vignetting. Then, contrast stretching is applied in order to enhance the intensity of wrinkles against skin. Denoising filters are applied to the image to reduce noise in the image. In the cell segmentation, extended-minima transform and watershed algorithm are used for cell-based segmentation. Each cell cluster is labeled, and the labeled information is utilized for calculating skin features. We extract five features from the skin image to analyze the skin condition.

The remainder of this paper is organized as follows. In Section II, we introduce several related works for skin analysis, wrinkle detection and cell segmentation. Detailed techniques for skin segmentation are described in Section III and skin feature extraction method is described in Section IV. We explain our experiment and conclude this paper in Section V.

II. RELATED WORKS

So far, medical analysis and diagnosis based on biometric images have been performed in the various domains. Skin analysis is one of the most popular and interesting tasks, since skin is the outermost part of the human body. Various methods for extracting diverse features from skin images and evaluating its condition quantitatively have been proposed.

As an effort to detect skin wrinkles, H. Tanaka et al. applied a cross-binarization method to digital skin image to get its binary image, and then, the short straight line matching method to detect wrinkles from the binary image and measure their length [4]. More specifically, for each base line in the

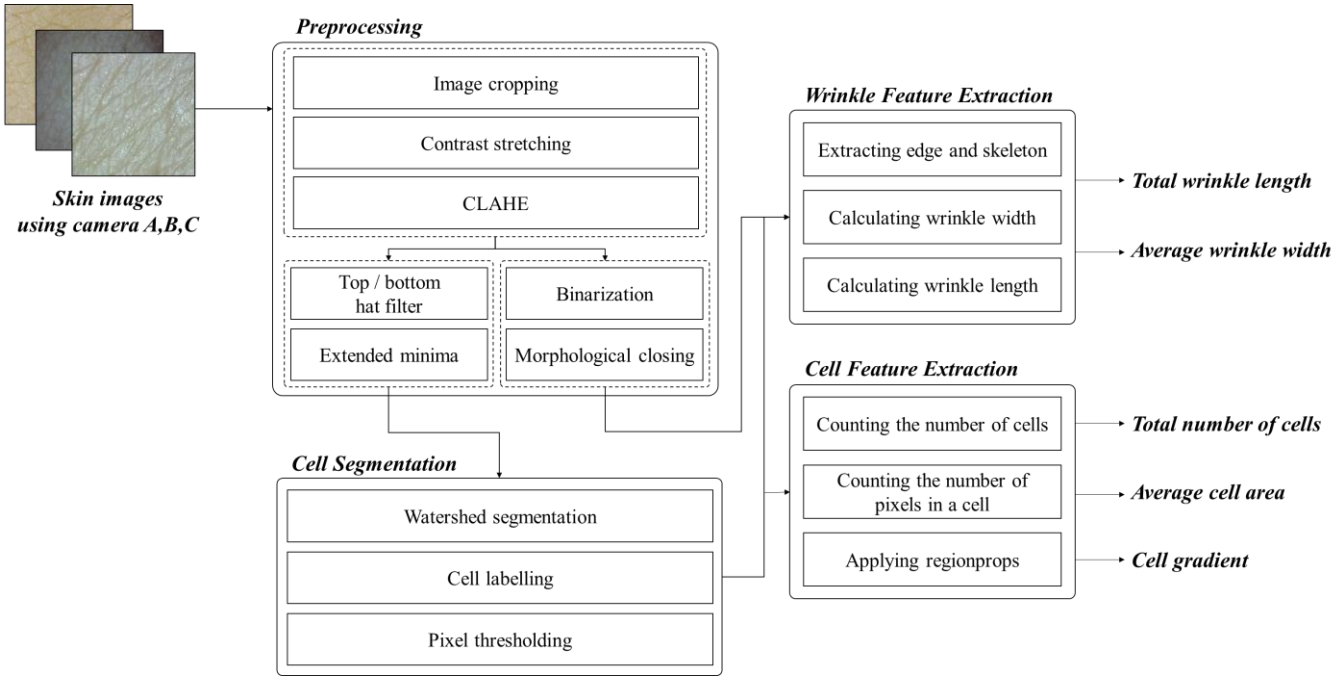

Figure 1. Overall scheme of skin feature extraction

cross-binarized image, if more than 70% of its pixels are marked black, then the line is considered a wrinkle. After that, they continue from the end of current base line to create a new base line. This repeats until the end of the wrinkle or the end of the image is reached. J. Ute et al. measured the topography of skin surface using an optical 3D device and showed that there is a significant dependency between skin surface topography and the age [5]. On the other hand, G. O. Cula et al. developed the automatic facial wrinkles detection algorithm based on estimating the orientation and frequency of the elongated spatial feature, captured via digital image filtering [6]. Recently Yow. Ai Ping et al. proposed the ASHIMA system framework and showed how to process HD-OCT (High-Definition Optical Coherence Tomography) skin images automatically to measure the epidermal thickness and skin surface topography [7]. H. Razalli et al. estimated human's age range based on facial wrinkle analysis [8]. They mentioned when fewer wrinkles are detected or extracted, it will consequently affect the process to estimate the correct age. To solve that, they proposed a new method to extract facial wrinkles in a face image using Hessian based filter (HBF) for age estimation. They tested their proposed method for FG-NET database and compared its performance with other methods.

One of the most popular algorithms for segmenting a skin microscope image into cells is watershed segmentation. Although it has been a long time since this algorithm was introduced, it is still widely used in various image processing applications. A. Das and D. Ghoshal segmented human skin region using watershed segmentation [9]. They converted RGB image into YCbCr color image, and then modified marker based watershed algorithm has been applied on Cr component for segmentation of human skin region. They compared their method with other algorithms. The methods were tested on FRI CVL Face Database. Z. JunXiong et al proposed a method for extracting features of jujube fruit wrinkle using the watershed segmentation [10]. They first converted original RGB image into gray scale image, and then, applied morphological reconstruction to remove noise. After that, they performed the H-minima extended transformation to label the foreground of jujube fruit images, and then segmented the labeled foreground regions using a distance transform-based watershed algorithm.

III. SKIN SEGMENTATION METHOD

A. Preprocessing

Direct image processing on microscope image or captured image might cause several problems if the image is in RGB (Red-Green-Blue) form. Usually, dealing with RGB image shows less accuracy than dealing with gray image. Other typical factors to decrease the accuracy are vignetting effect and noises. To avoid these problems, original images need to be converted into binary images through preprocessing. In this work, preprocessing consists of three steps: (i) the original image is cropped to reduce the effect of vignetting. (ii) Contrast stretching [11] is applied to make brightness difference between skin and wrinkle bigger. (iii) Adaptive histogram equalization is applied to the image. Figure 2 shows overall steps of preprocessing and their result on an example skin image.

1) Cropping

Due to the limitations of the camera and the interference of the light source, captured images may have a noise known as vignetting effect. Vignetting is a phenomenon where the

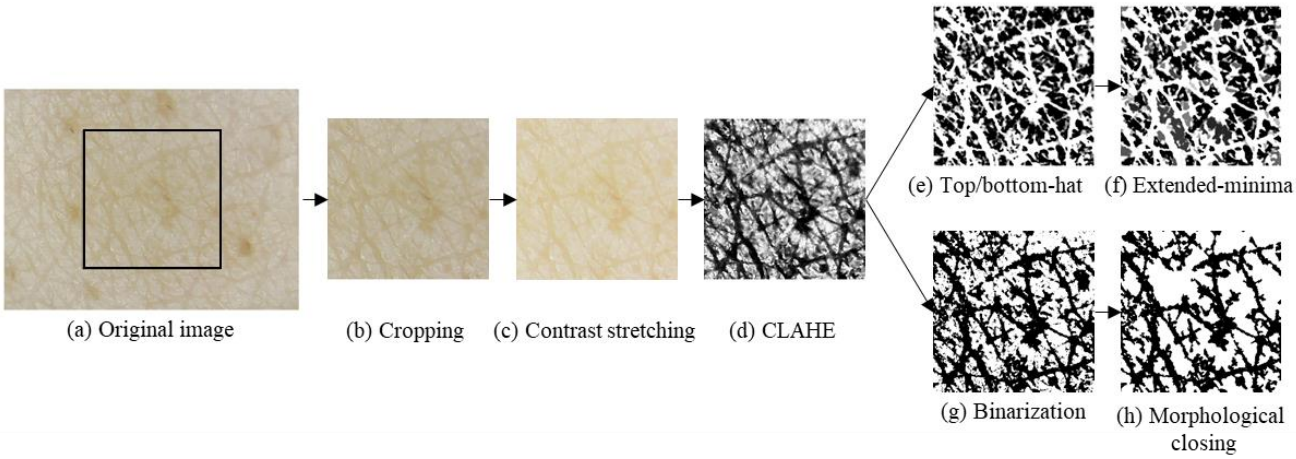

Figure 2. The example of overall preprocessing steps

outer edges of the images become dark due to the reduction of light at the periphery of camera lens, and as a result, the captured images have different color histogram distributions. An example of vignetting effect is shown in Figure 3, where we can see the dark area around the corner. In order to avoid such phenomenon, we cropped 300 by 300 pixels from the center of the image, which has the concentrated luminous source of the image. Figure 2 (b) shows the result of image cropping for an input image shown in Figure 2 (a), where the rectangle indicates the cropping size.

Figure 3. Example of vignetting effect

2) Contrast stretching

Accurate detection of skin wrinkles is very crucial in the skin analysis and the accuracy can be improved by clearly separating skin and wrinkle pixels in the image. However, original images often lack sufficient contrast depending on the conditions under which the image was photographed such as light source and shooting area. Insufficient contrast could make certain areas in the image have similar contrast even though they must be distinguished. This problem can be moderated by contrast stretching. Contrast stretching expands the dynamic range of the intensity levels so that it spans the color distance between skin and wrinkle. The equation of contrast stretching used in this paper is shown in Eq. (1).

$$V_{out} = \begin{cases} 0.6 \times V_{in} + 0.4, & V_{in} > \alpha \\ 0.25 \times V_{in}, & V_{in} < \beta \\ V_{in} = V_{in}, & Others \end{cases} \quad (1)$$

Here, V is a value in HSV domain and α and β are two constants calculated by Eq. (2). Other constants are obtained experimentally.

$$\alpha = \sqrt{\max(V) \times \min(V)}\,/V_{average}$$
$$\beta = \max(V) \times \sqrt{\max(V) \times \min(V)} \quad (2)$$

Figure 2 (c) shows the effect of contrast stretching for the cropped image. In the figure, we can see that the intensity of the skin pixels is reduced and the color distinction between skin and winkle becomes more prominent.

3) Contrast limited adaptive histogram equalization

Skin wrinkles can be detected using the watershed algorithm [12]. However, we observed that the algorithm couldn't detect all the wrinkles due to the lack of contrast. Hence, before we apply the watershed algorithm to the skin image, we need to enhance the intensity of winkles by using the contrast limited adaptive histogram equalization (CLAHE) method to the image [13]. Histogram equalization is a gray scale transformation used for contrast enhancement. It aims to get an image with uniformly distributed intensity levels over the whole intensity scale. In some case, the result of histogram equalization might be worse compared to the original image since the histogram of the resulting image becomes approximately flat. For instance, when high peaks in the histogram are caused by an uninteresting area, histogram equalization results in enhanced visibility of unwanted image area. This means that the local contrast requirement is not satisfied, and as a result, minor contrast differences are

entirely ignored when the number of pixels falling in a particular gray range is relatively small.

An adaptive method to avoid this drawback is block-based processing of histogram equalization [14]. In this method, an image is divided into sub-images or blocks, and histogram equalization is performed on each sub-images or blocks. Then, blocking artifacts among neighboring blocks are minimized by filtering or bilinear interpolation.

The CLAHE method uses a clip limit to overcome the noise problem. That is, the amplification is limited by clipping the histogram at a predefined value before computing the Cumulative Distribution Function (CDF). The value at which the histogram is clipped, the so-called clip limit, depends on the normalization of the histogram and thereby on the size of the neighborhood region. The redistribution will push some bins over the clip limit again, resulting in an effective clip limit that is larger than the prescribed limit.

In our work, we need to remove hairs from the gray image. Hairs can be mistaken for wrinkles and hence they are the most critical and common noise in the wrinkle detection. Skin hairs are easily removed by a simple threshold filter. Figure 2 (d) shows the result of the CLAHE method.

4) Binarization

In order to measure the width of wrinkles, we need to detect the contour of wrinkles and their skeleton. The contour and skeleton can be obtained by performing canny edge detection and morphological thinning [15][16]. They are effectively working on the binary image. Hence, we apply Otsu threshold to the resulting image of CLAHE method to obtain its binary image [17]. Figure 2 (g) shows the result of binarization.

5) Denoise

Even though CLAHE images and binarized images are ready for feature extraction, there are still likely to have some noises due to the hardware limitation or environmental factors when taking pictures. To reduce the effect of such noises, we perform a denoise process. We apply different denoise process to the CLACHE and binarized images, In the case of CLAHE image, top-hat, bottom-hat filter is applied to remove noise. Figure 2 (e) shows the result after applying top, bottom-hat filter. After filtering, Extended-minima transform and watershed segmentation are performed for cell segmentation. In the case of binarized images, morphological closing is performed to remove noise. Figure 2 (h) shows the result of morphological closing.

6) Extended-minima transform

Even though watershed transform is widely used for image segmentation, it often suffers from the over-segmentation problem since regional minima or ultimate eroded points are employed for segmenting cells directly. One of the key factors that determine the accuracy of skin image segmentation by wrinkle cells is how much the minima points are extended. In this paper, we revise the extended-minima transform, which is the regional minima of the H-minima transform. Regional minima are connected components of pixels with a constant intensity value, and whose external boundary pixels have higher value.

In other words, the result of h-minimum operator is linked to the depth of the minima. In a skin image, wrinkle cells consist of some minima and maxima. Minima correspond to parts of low depth points and maxima correspond to high depth points. Therefore, using the extended-minima transform, we can increase the depth between wrinkle cell clusters. It can help the watershed transform to cluster the wrinkle cells. First, we extract minima from an image and extend the depth of the points. Figure 2 (h) shows the result after imposing the extended minima to the original gray scale image.

B. Segmentation processing

In this section, we describe how to segment a skin image into wrinkle cells using the extended-minima transform [18] and watershed transform. Watershed transform is one of the most widely used image segmentation techniques in image processing and we use it for segmenting a skin image into wrinkle cells. Especially, we perform the extended-minima transform before the watershed transform in order to increase the accuracy of finding wrinkle cells.

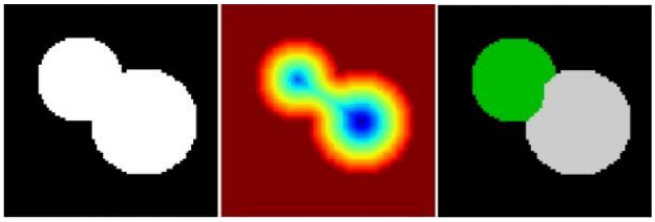

(a) Overlapping objects (b) Distances (c) Separated objects

Figure 4. Segmentation using watershed transform

1) Watershed segmentation

Image segmentation is a computer analysis of image objects to decide which pixel of the image belongs to which object. Basically, this is the process of separating objects from background, as well as from each other. Watershed transform is a powerful and well-known tool for performing image segmentation. Figure 4 shows how to segment two overlapping circles using the watershed transform.

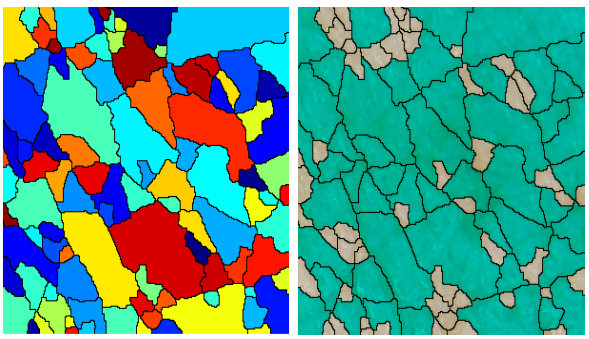

(a) Labeled image (b) Filtered image with valid cells

Figure 5. Labelling process

To segment them, an image distance to the background is computed. The maxima of the distance (i.e., the minima of the opposite of the distance) are chosen as markers, and the flooding of basins from such markers separates the two circles along a watershed line. We adapt these steps to our skin image, so that pixels of each wrinkle cell are clustered.

2) Cell labelling

Wrinkle cell labelling can be easily done by applying the watershed transform to the skin image. From the result of watershed transform, we can get a collection of wrinkle cells. Each cell contains the positions of the pixels in the cell which belong to same cluster. Figure 5 (a) shows an example of wrinkle cells labeling, where each cell is labeled using a different color.

3) Pixel thresholding

Sometimes, the segmentation result contains unexpected cells with very small size, which are usually noise or moles. Since they are not the regular wrinkle cells, they should be removed. We can calculate area of every labelled cell easily by counting the number of pixels in the cell. The threshold size by which we determine whether to remove the cell or not can be calculated by Eq. (3).

$$Threshold = \frac{\sum_i Area_i}{ScaleRatio \times n} \quad (3)$$

Here, $Area_i$ is the number of pixels in the ith cell and n is the total number of cells. Also, $ScaleRatio$ is defined by Eq. (4).

$$ScaleRatio = \frac{\max(Area) + \min(Area)}{mean(Area)} \quad (4)$$

Figure 5 (b) shows all the noisy cells detected by this method. We remove them by merging with their neighboring cell or enclosing cell.

IV. SKIN FEATURE EXTRACTION

A. Defining skin features

TABLE I. ASSUMPTIONS BASED ON COMMON KNOWLEDGE OF SKIN

1. Total wrinkle length decreases with age.
2. Wrinkle width increases with age.
3. Wrinkle depth increases with age.
4. Wrinkle cell area increases with age.
5. The number of cells decreases with age.
6. Diameter ratio of inscribed circle and circumscribed circle of a cell decreases with age.
7. Total length of lines connecting cross points of a cell increases with age.

We have developed algorithms for extracting various cell and wrinkle features from microscopy skin images. Our feature extraction method is based on the labeled image described so far. Before we describe our feature extraction scheme in detail, we first show several assumptions we made based on common knowledge of skin [2] in Table I.

In the table, the 6th assumption needs some explanation. Usually, each wrinkle cell has its own shape and the cell shape is getting distorted with aging. So, it might be helpful to evaluate how much a skin cell is distorted for skin aging estimation. In this paper, we represent the degree of distortion by the ratio of inscribed circle and circumscribed circle. Hence, if the cell's shape is very regular like regular polygon, the ratio approaches to 1. However, this method requires much processing time since it considers all the pixels in a cell. To alleviate this problem, we replace existing method with regionprops. This method considers how irregular a cell shape is based on the angle instead of the ratio of radius length. In other words, we consider the slope of principal horizontal axis as the distortion degree of a cell.

Finally, we define five skin features for skin aging estimation. They are cell count, average cell area, average cell gradient, total wrinkle length, and average wrinkle width. Cell count indicates how many cells are in the skin image. Average cell area indicates the average area of cells in the skin image. Cell gradient is what we described above,

The wrinkle itself is a very important clue for estimating the degree of skin aging. We use two wrinkle features in this work; the total wrinkle length and the average wrinkle width. We will describe detailed steps for extracting these features in the following.

B. Calculating skin features

In this section, we describe how to calculate five skin features. At first, the number of cells can be easily obtained by counting the number of labeled cells while excluding cells with invalid size as we described earlier.

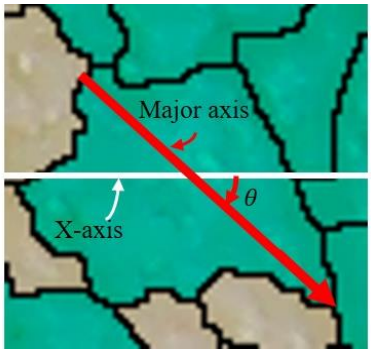

Figure 6. Example of calculating angle

The average cell area is also simply calculated by dividing the total number of pixels in the labeled cells by the number of cells which we obtained in the first place. In order to calculate the cell gradient, we used the regionprops function [19] which calculates a set of features for each labeled region.

(a) A binary image (b) Its skeleton image (c) Contour image (d) Skeleton + contour

Figure 7. Extracting wrinkle skeleton and contour

One of the major features in the result of regionprops is the scalar angle value for each labeled region. It can be obtained by calculating the angle between the x-axis and the major axis of the ellipse that has the same second-moment as the region. Figure 6 illustrates how to calculate the angle. In the Figure, white line describes x-axis and red arrow shows a major axis. The angle between these two lines is calculated by regionprops method.

Total wrinkle length can be calculated using the line sieving method. This method first counts the pixels on the horizontal and vertical texture lines. It then counts the pixels along the diagonal line, and estimates the actual wrinkle length considering its slope. In the case of single pixel islands on the image, we simply count these islands and add the number to the total length.

To calculate average wrinkle width is a little complicated compared with other features. Figure 7 shows overall steps for to obtaining wrinkle width. We first apply morphological thinning on binary image. Thinning is a morphological operation that removes foreground in overall binary image. Figure 7 (b) shows the result of morphological thinning on the original image in Figure 7 (a). It consists of a set of 1x1 pixel points called skeleton. These pixels have specific direction, thus we can calculate each point's direction. In order to calculate the direction, we used Principal Component Analysis (PCA) algorithm [20]. PCA algorithm is a method of calculating Eigen value and Eigen vector by using all data's covariance and average.

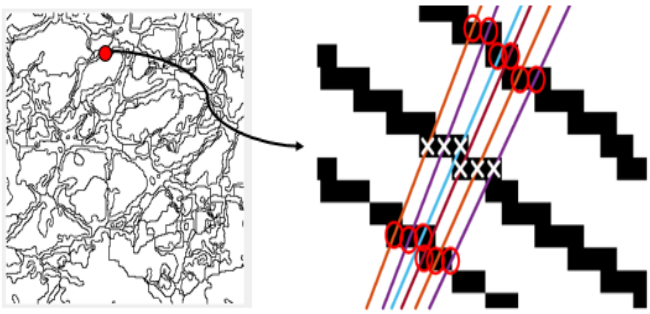

Figure 8. Calculating wrinkle width

Using this algorithm, we can get all of points on the skeleton's direction. Then, we can get a perpendicular line for each point. After calculating perpendicular lines, we can get the wrinkle contour by using canny edge detection. Figure 7 (c) shows the wrinkle contour detected by using canny edge detection. Finally, we can merge the skeleton and contour together as shown in Figure 7 (d). When aforementioned processes are done, we can calculate its wrinkle width. Figure 8 shows how to calculate average wrinkle thickness. The left image in the figure is merged image of wrinkle skeleton and contour as shown in Figure 7 (d). The right image magnifies a specific point of the image. In the figure, each white '×' is skeleton point, and the line passing the skeleton point is a normal line. The red circles indicate the intersection of line and wrinkle contour. The length between these two intersection points is the wrinkle thickness at that point.

(a) Camera A (b) Camera B

(c) Camera C

Figure 9. Microscopy cameras compatible with smartphone

(a) Original cropped image (b) Ground truth (c) Removed skin area (d) Proposed method (e) Overlapping

Figure 10. Evaluation of cell detection accuracy

V. EXPERIMENTS

In order to evaluate the performance of our revised scheme, we performed several experiments based on the Matlab 2016a. To collect skin images, we used three different microscopy cameras shown in Figure 9, which are easily connected with smartphone. The reason we used different cameras is that images show quite different characteristics depending on the camera. Hence, to see the robustness of our method, we decided to test diverse cameras.

The scales of the cameras A, B, and C are 50X to 500X, 25X to 400X and 60X, respectively. In our previous work, we used the camera C only. We got approximately 300 face skin images and 60 hand skin images.

In our previous work, we evaluated the accuracy of our revised method by matching binary image pixel and cell contour [1]. In that case, we consider binary image as ground truth. However, sometimes binary image is not appropriate for use as ground truth. A typical case is when the original image contains various unexpected characteristics such as noise, mole, and light reflection. To solve this problem, we have made the ground truth manually. In the evaluation, we focused on two tasks: wrinkle line detection and cell detection. Numerical data for some of the experimental results are shown in Table II. More detailed analysis of the results is described in the next Section.

TABLE II. NUMERICAL DATA FOR EXPERIMENTAL RESULT

	Sub 1	*Sub 2*	*Sub 3*	*Sub 4*	*Sub 5*	*Sub 6*	…	*AVERAGE*
Face Wrinkle-CAMERA A-Revised method	96.512	97.11	97.362	94.912	95.334	96.112	…	96.520
Face Wrinkle-CAMERA A-Previous method	88.905	87.013	90.288	89.991	86.032	84.950	…	86.276
Face Wrinkle-CAMERA B-Revised method	95.748	96.869	97.390	97.938	96.381	96.920	…	96.837
Face Wrinkle-CAMERA B-Previous method	84.897	85.647	85.327	88.739	85.773	87.137	…	86.389
Face Wrinkle-CAMERA C-Revised method	95.720	96.801	95.147	94.510	94.490	96.400		95.912
Face Wrinkle-CAMERA C-Previous method	89.604	89.585	91.200	90.073	89.979	91.369	…	89.781
Hand Wrinkle-CAMERA A-Revised method	96.456	97.957	95.095	97.016	97.476	96.094	…	97.260
Hand Wrinkle-CAMERA A-Previous method	87.967	89.220	89.837	91.700	88.448	89.302	…	89.115
Hand Wrinkle-CAMERA B-Revised method	97.021	95.170	96.664	95.308	97.943	96.215	…	97.103
Hand Wrinkle-CAMERA B-Previous method	88.935	88.290	89.139	88.235	89.325	89.574	…	88.835
Hand Wrinkle-CAMERA C-Revised method	97.015	97.109	95.165	96.463	98.658	96.231	…	97.303
Hand Wrinkle-CAMERA C-Previous method	91.888	91.051	92.364	88.966	90.729	89.719	…	90.927
Face Wrinkle-CAMERA A-Revised method	98.520	97.437	97.991	95.554	96.143	96.340	…	96.612
Face Wrinkle-CAMERA A-Previous method	86.353	84.977	85.957	83.203	84.901	84.431	…	85.255
Face Wrinkle-CAMERA B-Revised method	94.966	97.051	96.825	96.576	95.209	97.670	…	96.543
Face Wrinkle-CAMERA B-Previous method	83.696	83.047	83.369	83.084	81.596	83.060	…	83.346
Face Wrinkle-CAMERA C-Revised method	96.304	96.156	95.979	96.601	95.132	98.099	…	97.135
Face Wrinkle-CAMERA C-Previous method	87.754	87.214	87.199	86.436	88.253	87.101	…	87.234
Hand Wrinkle-CAMERA A-Revised method	96.193	98.259	96.683	96.319	96.614	96.060	…	96.908
Hand Wrinkle-CAMERA A-Previous method	88.245	91.891	91.020	89.673	88.108	88.500	…	89.365
Hand Wrinkle-CAMERA B-Revised method	97.057	98.025	95.902	94.904	95.785	97.568	…	97.234
Hand Wrinkle-CAMERA B-Previous method	89.596	89.657	89.075	89.389	88.729	90.067	…	89.205
Hand Wrinkle-CAMERA C-Revised method	96.427	98.244	96.940	97.454	98.342	98.828	…	97.789
Hand Wrinkle-CAMERA C-Previous method	90.128	92.507	91.906	91.178	91.051	91.028	…	91.246

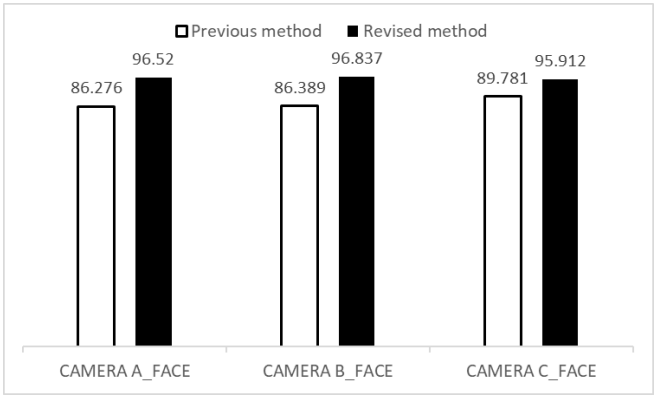

(a) Accuracy of face wrinkle line detection

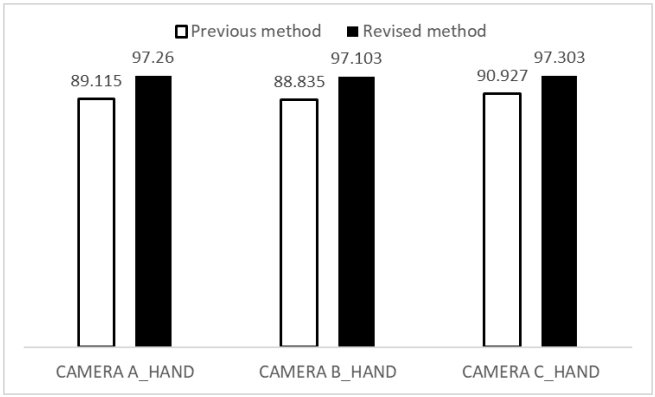

(b) Accuracy of hand wrinkle line detection

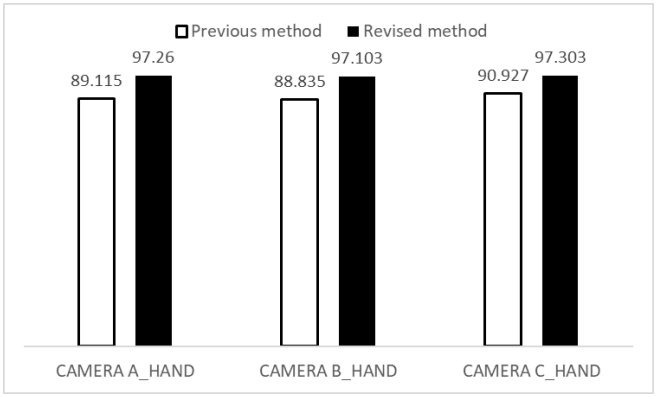

(c) Accuracy of face cell detection

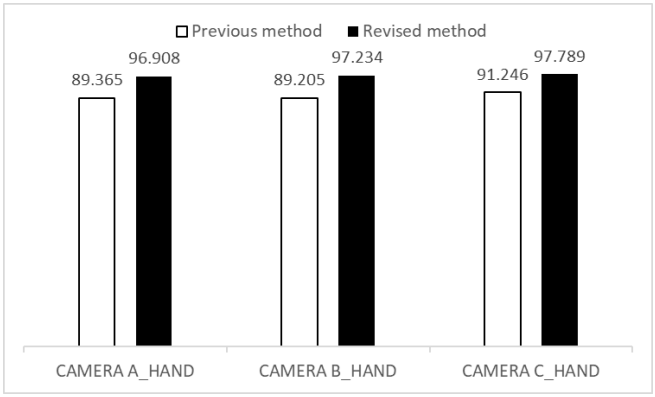

(d) Accuracy of hand cell detection

Figure 11. Accuracy comparison

A. *Wrinkle line detection accuracy*

To evaluate the accuracy of wrinkle detection, we made ground truth manually using all the images captured using three cameras. That is, we identified and marked cell boundaries (wrinkle) with eyes.

Figure 10 shows an example. Figure 10 (a) shows an original image of 300x300 pixel. Figure 10 (b) shows all the manually identified wrinkle lines on the skin image, and Figure 10 (c) shows only wrinkle lines. On the other hand, Figure 10 (d) shows all the wrinkle lines detected by our proposed method. The detection accuracy can be confirmed visually by overlapping Figure 10 (c) and Figure10 (d) as shown in Figure 10 (e) and quantitatively measured by using Eq. (5).

$$Accuracy = \frac{NWP \cap WP_{GT}}{NWP} \times 100 \qquad (5)$$

Here, NWP is the number of wrinkle pixels and WP_{GT} is the number of pixels on the wrinkle lines in the ground truth.

Basically, the equation counts those pixels that exist on both wrinkle lines, and then they are divided by the total number of pixels on the cell contour lines.

Figure 11 compares the accuracy of our previous method and revised method on the face and hand skin images. From the figure, we can see that our revised method achieved higher accuracy compared to the previous method.

Moreover, our revised method is more robust in hardware characteristics. For instance, Figure 12 shows the result of wrinkle detection on the facial and hand skin using three different cameras. As shown in the figure, our previous method showed different but poor performance depending on camera. However, our revised method showed good and consistent performance regardless of camera.

B. *Cell detection*

To evaluate the accuracy of cell detection, we used the same ground truth that we mentioned in the last section as follows. If the cell detected by our revised method has a similar location with some cell in the ground truth and the ratio of the cell pixels over the ground truth cell is more than

80%, we declare the cell correctly detected. The accuracy of cell detection is compared in Figure 11 (c) and (d). The accuracy is a little lower compared to the wrinkle detection accuracy. This is because in the case of cell detection, all pixels need to be matched

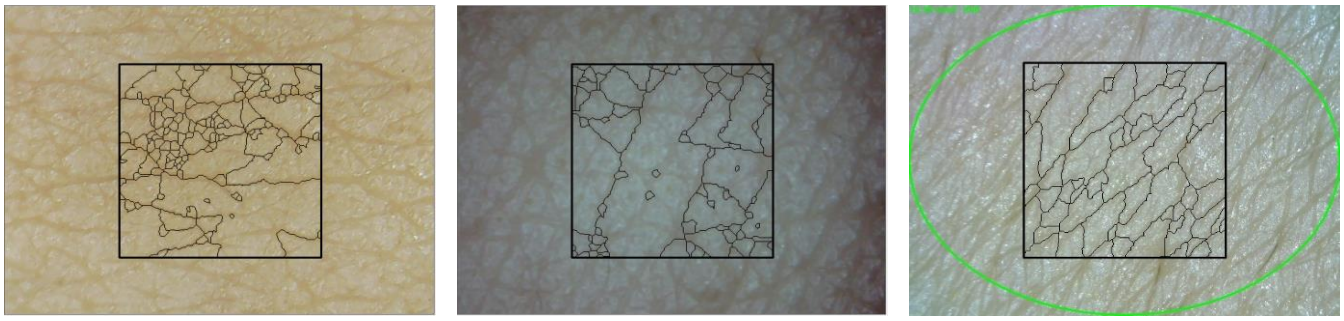

(a) Camera A and previous method (b) Camera B and previous method (c) Camera C and previous method

(d) Camera A and revised method (e) Camera B and revised method (f) Camera C and revised method

Figure 12. Robustness comparison

C. Execution time

Next, we compare the execution time of our previous and revised methods spent for cell detection. Here, total execution time consists of preprocessing time, cell segmentation time and feature extraction time. Figure 13 compares the execution time of previous method and revised method spent for analyzing one skin image. In the figure, both methods have very similar segmentation time since they use same segmentation method. But, we can see considerable reductions in the preprocessing time and feature extraction time. Especially, feature extraction time has been reduced to more than 1/3 by removing pixel-based computation. This reduction is very critical since feature extraction time occupies considerable part of total execution time. As a result, our revised method has reduced the execution time by half compared with the previous method.

VI. CONCLUSION

In this paper, we revised our method for skin feature extraction to improve its accuracy, efficiency and robustness. To improve the accuracy of skin cell detection, we enhanced the contrast of wrinkles on the skin by using the contrast limited adaptive histogram equalization (CLAHE) and highlighted the depth of wrinkles by using the extended-minima transform. In the experiments, we collected skin images using diverse cameras and measured the accuracy and execution time. The result shows that the performance has improved twice in terms of execution time and the accuracy also has improved by 10%. In addition, the performance was not affected much by the camera type, which shows the robustness of our method.

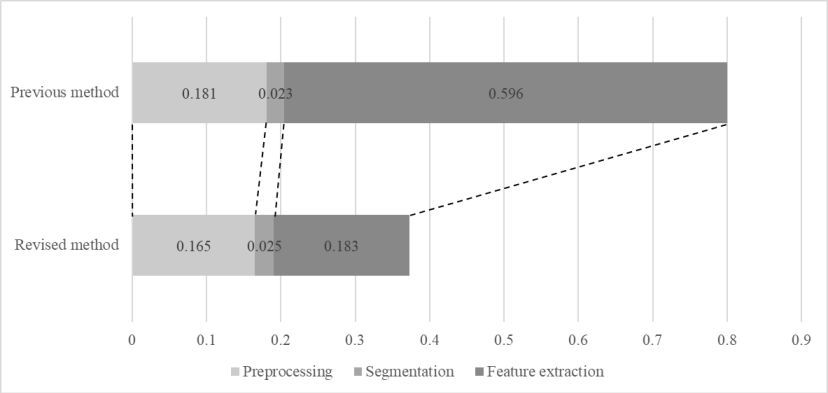

Figure 13. Comparison of excution time

ACKNOWLEDGEMENT

This work was supported by Institute for Information & communications Technology Promotion (IITP) grant funded by the Korea government (MSIP) (No. R0190-16-2012, High Performance Big Data Analytics Platform Performance Acceleration Technologies Development).

REFERENCES

[1] W. Kim, H. Kim, and E. Hwang, “Improving Feature Extraction Accuracy for Skin Analysis,” The Ninth International Conferences on Advances in Multimedia, pp. 26-31, April 2017.

[2] Y. H. Choi, D. Kim, E. Hwang, and B. Kim, "Skin texture aging trend analysis using dermoscopy images," Skin Research and Technology, vol. 20, no. 4, pp. 486-497, 2014.

[3] Y.-H. Choi, Y.-S. Tak, S. Rho, and E. Hwang, "Skin feature extraction and processing model for statistical skin age estimation," Multimedia tools and applications, vol. 64, no. 2, pp. 227-247, 2013.

[4] H. Tanaka et al., "Quantitative evaluation of elderly skin based on digital image analysis," Skin research and technology, vol. 14, no. 2, pp. 192-200, 2008.

[5] U. Jacobi et al., "In vivo determination of skin surface topography using an optical 3D device," Skin Research and Technology, vol. 10, no. 4, pp. 207-214, 2004.

[6] G. O. Cula, P. R. Bargo, A. Nkengne, and N. Kollias, "Assessing facial wrinkles: automatic detection and quantification," Skin Research and Technology, vol. 19, no. 1, pp. e243-e251, 2013.

[7] A. P. Yow et al., "Automated in vivo 3D high-definition optical coherence tomography skin analysis system," in Engineering in Medicine and Biology Society (EMBC), 2016 IEEE 38th Annual International Conference of the, pp. 3895-3898, 2016.

[8] Razalli, et al., "Age Range Estimation Based on Facial Wrinkle Analysis Using Hessian Based Filter," Advanced Computer and Communication Engineering Technology, Springer International Publishing, pp. 759-769, 2016.

[9] A. Das and D. Ghoshal, "Human Skin Region Segmentation Based on Chrominance Component Using Modified Watershed Algorithm," Procedia Computer Science, 89, pp. 856-863, 2016.

[10] R. C. Gonzalez and R. E. Woods, “Digital Image Processing,” Addison-Wesley, Third edition, 2008.

[11] Z. Junxiong, M. Qingqin, L. Wei, and X. Tingting, "Feature extraction of jujube fruit wrinkle based on the watershed segmentation," International Journal of Agricultural and Biological Engineering, vol. 10, no.4, pp.165-172, 2017

[12] L. J. Belaid and W. Mourou, "Image segmentation: a watershed transformation algorithm," Image Analysis & Stereology, vol. 28, no. 2, pp. 93-102, 2011.

[13] Pizer, et al., "Contrast-limited adaptive histogram equalization: speed and effectiveness," in Visualization in Biomedical Computing, Proceedings of the First Conference on, pp. 337-345, 1990.

[14] Y. C. Hum, K. W. Lai, and M. I. Mohamad Salim, "Multiobjectives bihistogram equalization for image contrast enhancement," Complexity, vol. 20, no. 2, pp. 22-36, 2014.

[15] J. Canny, “A computational approach to edge detection,” IEEE Transactions on Pattern Analysis and Machine Intelligence, Vol. 8, No. 6, pp. 679-698, 1986.

[16] L. Lam, S. W. Lee, and C. Y. Suen, “Thinning Methodologies-A Comprehensive Survey,” IEEE Transactions on Pattern Analysis and Machine Intelligence, Vol 14, Issue 9, pp. 879, 1992.

[17] N. Otsu, "A threshold selection method from gray-level histograms," Automatica, vol. 11, no. 285-296, pp. 23-27, 1975.

[18] P. Soille, Morphological image analysis: principles and applications. Springer Science & Business Media, 2013.

[19] A. Othmani, et al., "Region-based segmentation on depth images from a 3D reference surface for tree species recognition," Image Processing (ICIP), 2013 20th IEEE International Conference on. IEEE, pp. 3399-3402, 2013.

[20] S. Wold, K. Esbensen, and P. Geladi, "Principal component analysis," Chemometrics and intelligent laboratory systems, vol. 2, no. 1-3, pp. 37-52, 1987.